Nickel Enhances InPd-catalyzed Nitrate Reduction Activity and N_2 Selectivity

Kiheon Hong,[1,2] Daniel J. Rivera,[2,3] Juan Donoso,[2,4] Bongki Shin,[5] Hunter P. Jacobs,[4,6] Byeong Jun Cha,[4] Kimberly N. Heck,[4] Welman C. Elias,[4] Paul Westerhoff,[2,7] Yimo Han,[5] Christopher Muhich,[2,3] Michael S. Wong[1,2,4,5,8,9,10*]

[1]Department of Civil and Environmental Engineering, Rice University, 6100 Main Street, Houston, TX 77005, USA
[2]Nanosystems Engineering Research Center for Nanotechnology-Enabled Water Treatment, 6100 Main Street, Houston, TX 77005, USA
[3]Chemical Engineering Program, School for Engineering of Matter, Transport and Energy, Arizona State University, Tempe, AZ 85281, USA
[4]Department of Chemical and Biomolecular Engineering, Rice University, 6100 Main Street, Houston, TX 77005, USA
[5]Department of Materials Science and NanoEngineering, 6100 Main Street, Houston, TX 77005, USA
[6]Manufacturing Science Division, Oak Ridge National Laboratory, 1 Bethel Valley Road, Oak Ridge, TN 37830, USA
[7]School of Sustainable Engineering and the Built Environment, Arizona State University, Tempe, AZ, 85287-3005, USA
[8]Department of Chemistry, Rice University, 6100 Main Street, Houston, TX 77005, USA
[9]Rice Water Institute, Rice University, 6100 Main Street, Houston, TX 77005, USA
[10]Rice Advanced Materials Institute, Rice University, 6100 Main Street, Houston, TX 77005, USA

*Email: mswong@rice.edu

KEYWORDS. nitrate reduction, trimetallic catalyst, palladium, nickel, cost

Abstract

Palladium-indium (PdIn) is a well-established bimetallic composition for reductively degrading nitrate anions, one of the most ubiquitous contaminants in the groundwater. However, the scarcity and the variable price of these rare earth and platinum group critical metals may hinder their use for water treatment. Nickel (Ni), a non-precious metal in the same element group as Pd, could partially replace and lower Pd usage if the resulting trimetallic composition is sufficiently catalytically active. Herein, we report the synthesis and nitrate reduction catalysis of activated carbon-supported "In-on-Pd-on-Ni" catalysts (InPdNi/AC). Whereas bimetallic InPd/AC (0.05 wt% In, 1.3 wt% Pd) was expectedly active, trimetallic InPdNi/AC containing the same In amount, much less Pd (0.1 wt%), and 1 wt% Ni, was >17 more active (k_{cat} ≈ 20 *vs.* 349 $Lmin^{-1}g_{surface\text{-}metal}^{-1}$). X-ray photoelectron spectroscopy (XPS) and density functional theory (DFT) calculations showed that Pd gained electron density from the Ni, correlating to the increased nitrate reduction activity. Ammonium by-product selectivity for InPdNi/AC (18% at 50% nitrate conversion) was lower compared to that of InPd/AC (48%), suggestive of higher surface coverage of NO or its greater reactivity with NO_2^- which lead to more N_2. Accounting for catalyst precursor, manufacturing costs, and spent metal recovery, we calculated that Ni incorporation lowered net catalyst cost significantly (from $1028/kg to $170/kg). The trimetallic composition lowered, by ~26 times, the catalyst cost of a stirred tank reactor sized to the same treatment capacity as that for the bimetallic case. The results demonstrate the partial replacement of the precious metal with an earth-abundant one leads to both a higher-efficiency and a lower-cost denitrification catalyst, via a materials strategy that should be beneficial for other clean-water catalytic systems.

Introduction

Nitrate (NO_3^-) contamination in groundwater has been a pervasive problem and it is expected to grow even more as the demand for agricultural fertilizer use increases and new health risks are identified.[1,2] Acute exposure to NO_3^- and its reduced form, nitrite (NO_2^-), can cause serious health problems, such as blue-baby syndrome (methemoglobinemia). Current United States Environmental Protection Agency (U.S. EPA) limits the maximum contaminant level (MCL) of NO_3^- and NO_2^- to 10 and 1 mg-N/L, respectively.[3] Cancer and hypertension continue to be evaluated as additional health endpoints with the potential to reduce regulatory limits in the future.[4–6]

Technologies including ion exchange (IX), reverse osmosis, biological treatment, and electrodialysis remove NO_3^- in drinking water at smaller and larger scales.[7–12] Of these physical removal technologies, IX is the most commonly used to treat NO_3^- in the U.S.[7,9] However, its main drawback (like the other processes) is that after IX resin regeneration it produces NO_3^- concentrated waste brines up to 20 wt% NaCl containing nitrate, sulfate and bicarbonate.[13] While anaerobic biological treatment is common for wastewater treatment, it is not used for drinking water treatment. The requirements of adding external organic (*e.g.*, acetic acid) or inorganic (*e.g.*, hydrogen gas) electron donors limit its full-scale adoption because of challenges due to active biomass growth during intermittent system operations and release of extracellular byproducts into the treated drinking water.[14–19]

NO_3^- electroreduction has also been considered as an alternative for converting NO_3^- into N_2 gas in both drinking water and wastewater treatment as electroreduction process has great potential to effectively remove NO_3^-.[20–25] However, achieving selective NO_3^- reduction to N_2 becomes challenging when treating water with low NO_3^- concentration, which is commonly found in groundwater.[26] Furthermore, the addition of electrolytes and chloride ions, along with the requirement to maintain a high pH for effective removal, significantly limits the applicability of using electrocatalytic reduction of NO_3^- in drinking water treatment applications.[26,27]

Another emerging destructive approach is catalytic reduction. Since the first publication of bimetallic palladium(Pd)-based NO_3^-/NO_2^- reduction in 1989 by Vorlop and Tacke,[28] there

have been significant efforts to understand the reduction chemistry, to improve the catalytic materials, and to develop them into a viable technology.[29–39] Although monometallic Pd is an excellent reduction catalyst for NO_2^-, it is ineffective for NO_3^- reduction.[28,29,40,41] An appropriately chosen second metal is needed to promote NO_3^- reduction. In 1997, Vorlop and coworkers reported a PdIn bimetallic catalyst for NO_3^- reduction for the first time, where In activates the reduction of NO_3^- to NO_2^-, and Pd is responsible for the subsequent reduction of NO_2^- to the end product, either N_2 or NH_4^+.[42] The PdIn combination is preferred for NO_3^- reduction over PdCu and PdSn compositions due to higher by-product selectivity towards N_2 over NH_4^+,[32,36,37,42–44] and catalyst stability under various reaction conditions.[45,46]

Our group showed in 2018 that (i) In-decorated Pd nanoparticles are catalytically active for NO_3^- reduction, (ii) their NO_3^- reduction activity show a strong volcano-shape dependence on In surface coverage, (iii) the most active PdIn composition contain two-dimensional ensembles of 4-6 indium atoms, and (iv) the In metal undergoes room-temperature oxidation in the presence of NO_3^- species and H_2-driven reduction during the NO_3^- reduction reaction.[36] Through rational control of the materials composition and structure, we showed enhanced catalysis when gold was incorporated[47] and when cube-shaped Pd nanoparticles were used to support the In metal.[37]

PdIn catalysis can be actualized in several treatment approaches, for example, in a capacitive deionization flow system as a magnetically responsive dispersion,[48] and in metal catalytic film reactor equipped with hydrogen-permeable hollow fibers.[49] Problematically, the scarcity and volatile price of the precious metal hinder the implementation of Pd-based catalytic NO_3^- treatment.[22]

We suggest that Pd metal usage can be dramatically lowered by replacing a fraction of the precious metal Pd with the base metal Ni (another Group 10 element that is a less costly metal) in the form of a PdNi bimetallic composition. Hörold *et al.* (1993) and Soares *et al*. (2008) reported that PdNi exhibited very low activity for NO_3^- reduction, with a very high ammonium selectivity.[41,50] Besides these works, we are unaware of other reports on this bimetallic composition for NO_3^- (or NO_2^-) reduction. Other PdNi catalyzed reactions have been

studied demonstrating enhanced performance for reactions, such as electrocatalytic oxidation, hydrogenation of organic compounds, and carbon-coupling reactions.[51–58] We hypothesize that PdNi, under proper synthesis conditions and with the addition of In metal as a promoter, would be active for NO_3^- reduction.

In this work, we synthesized trimetallic catalysts by sequentially depositing Ni, Pd, and In on activated carbon ("InPdNi/AC"). We selected AC as the support material because of its relative inertness, high surface area, stability under both acidic and basic reaction conditions, and the presence of oxygen-rich functional groups which can mitigate severe metal agglomeration.[30,59,60] We assessed their NO_3^- reduction activity in comparison with bimetallic InPd ("InPd/AC") and monometallic catalysts, by comparing the initial reaction rate constants normalized to surface metal content. We examined the origin of the enhanced catalysis through x-ray diffraction (XRD), scanning transmission electron microscopy (STEM), CO chemisorption, and x-ray photoelectron spectroscopy (XPS). In addition, we conducted an estimation of catalyst cost via the CatCost software[61] and quantified the operating cost savings that stem from the higher activity and lower catalyst cost of InPdNi/AC compared to InPd/AC.

2. Materials and Methods

2.1. Materials

Nickel(II) chloride hexahydrate ($NiCl_2{\cdot}6H_2O$, >95%), potassium tetrachloropalladate(II) (K_2PdCl_4, >98%), indium(III) chloride tetrahydrate ($InCl_3{\cdot}4H_2O$, >97%), potassium nitrate (KNO_3, > 99%) were purchased from Sigma Aldrich. Hydrogen gas (H_2, 99.999%), carbon dioxide gas (CO_2, 99.995%), dinitrogen gas (N_2, 99.999%), argon gas (Ar, 99.999%), diluted hydrogen gas in argon (10%H_2/Ar), and diluted carbon monoxide gas in helium (10%CO/He) were purchased from Airgas. Activated carbon (AC, G-60, ~100 mesh, specific surface area 500 – 1000 m^2/g) was purchased from Darco. All experiments were conducted using deionized (DI) water (>18.2 MΩcm, Barnstead NANOpure Diamond). Deaerated deionized (DDI) water was prepared by purging N_2 for 15 min. Pd stock solution (5 g-Pd/L) and In stock solution (2 g-In/L) were prepared by dissolving 460.1 mg K_2PdCl_4 and 153.2 mg $InCl_3{\cdot}4H_2O$, respectively,

in 30 mL DI water. Lastly, NO_3^- stock solution (5 g-NO_3^-/L) was prepared by dissolving 244.6 mg KNO_3 in 30 mL DI water.

2.2. Catalyst Synthesis

2.2.1. Ni/AC Catalyst

Ni metal supported on AC was prepared via wetness impregnation of AC, with a target Ni loading of 1.0 wt%. 163.63 mg of $NiCl_2 \cdot 6H_2O$ were dissolved in 5 mL of DI water and slowly dripped into an AC suspension (4 g of AC and 15 mL of DI water) and stirred for 12 h at 300 rpm. The resulting material was not filtered, but rather, the resulting suspension was oven dried at 80 °C overnight. The dried powder was then heated under H_2 at 550 °C for 3 h (after a ramp rate of 35 °C/min), cooled to room temperature, and purged out the H_2 with Ar gas for 15 min before taking out the sample. The final material was termed "Ni1.0/AC".

2.2.2. PdNi/AC Catalyst

"PdNi/AC" was prepared via wetness impregnation of Ni1.0/AC, with a target Pd loading of 0.3 wt%. 1.0 g of Ni1.0/AC was suspended in 15 mL of DDI water, purged with N_2 at 100 mL/min flow for 15 min to deoxygenate, and stirred at 600 rpm in a septum-sealed 40-mL bottle. Then 0.599 mL Pd stock solution was injected, and the mixture was stirred for 30 min under bubbling N_2 (100 mL/min). Afterwards, the solid was separated from the solution through centrifugation and dispersed in ethanol; this washing procedure was carried out a total of three times. Finally, the sample was vacuum-dried in an oven at 60 °C overnight (Scheme 1).

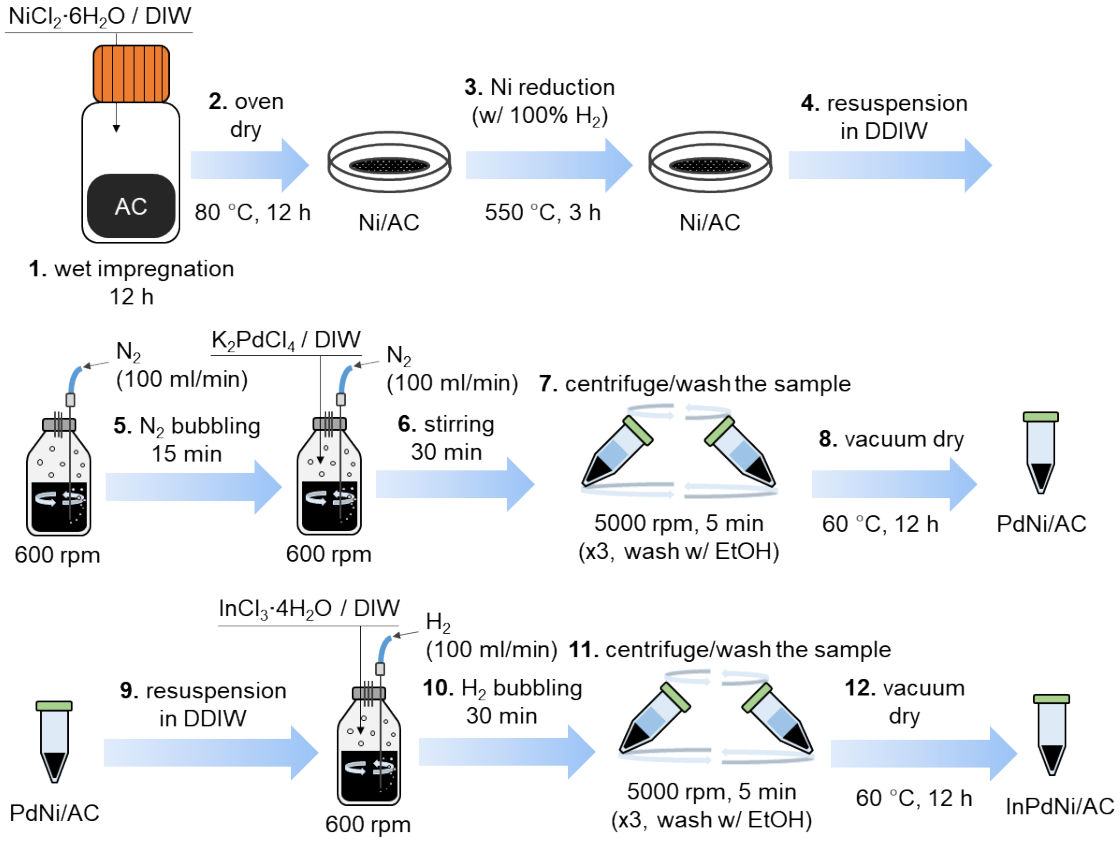

Scheme 1. Illustration of synthesis steps for InPdNi/AC

2.2.3. InPdNi/AC Catalyst

InPdNi/AC with a target loading of 0.05 wt% In was prepared using PdNi/AC (Scheme 1). The In addition assumes that all the In precursor is fully reduced onto the Pd surface.[36] 0.5 g of PdNi/AC was suspended in 15 mL of DDI water, bubbled with H_2 at 100 ml/min flow for 15 min to reduce any oxidized surface Pd, and stirred at 600 rpm. Then 144 µL of In stock solution was injected into the synthesis flask and stirred for another 30 min. Afterwards, the solid was separated, washed, and dried as described in the Section 2.2.2.

2.2.4. Other Catalyst Compositions

Bimetallic InPd metal supported on AC was synthesized for the comparison. First, Pd metal supported on AC was prepared via wetness impregnation of AC, with a target Pd loading of 0.3 and 1.3 wt%. 1.581 and 0.361 mL of Pd stock solution was slowly dripped into an AC

suspension (0.6 g of AC and 15 mL of DI water) and stirred for 12 h at 300 rpm. The resulting suspension was oven dried at 80 °C overnight. The dried powder was then heated under H_2 at 150 °C for 1 h (ramp rate of 15 °C/min), cooled to room temperature, and purged out with Ar gas for 15 min before taking out the sample. The materials were termed "Pd0.3/AC" and "Pd1.3/AC".

"InPd0.3/AC" and "InPd1.3/AC" were prepared by adding In stock solution and bubbling H_2, simultaneously, to Pd0.3/AC and Pd1.3/AC. 0.5 g of Pd0.3/AC and Pd1.3/AC catalysts were suspended in 15 mL of DDI water, bubbled with H_2 at 100 ml/min flow for 15 min to reduce any oxidized surface Pd, and stirred at 600 rpm. Subsequently 127 and 125 µL of In stock solution, respectively, was injected to coat In on Pd and stirred for another 30 min. Afterwards, the solid was separated, washed, and dried as described in the Section 2.2.2.

Bimetallic InNi supported on AC was prepared with a target In loading of 0.05 wt%. 0.5 g of Ni1.0/AC was suspended in 15 mL of DDI water, purged with H_2 at 100 mL/min flow for 15 min and stirred at 600 rpm in a septum-sealed 40-mL bottle. Then 125 µL of In stock solution was injected, and the mixture was stirred for 30 min under bubbling H_2 (100 mL/min). Afterwards, the solid was separated, washed, and dried as described in the Section 2.2.2.

2.3. Catalyst Characterization

N_2 adsorption isotherms were obtained using an Autosorb-iQ-MP and conducted at the temperature of liquid-N_2 (-196.2 °C). Prior to the measurements, the sample underwent a 12 h degassing process under vacuum conditions at approximately 2 mmHg at 200 °C. The surface areas were determined by applying the Brunauer-Emmett-Teller (BET) model.

High-angle annular dark-field scanning transmission electron microscopy (HAADF-STEM) imaging and energy dispersive X-ray spectroscopy (EDX) elemental mapping were performed using a Thermo Scientific Titan Themis3 at an acceleration voltage of 300 kV. Prior to use, TEM grids (ultrathin carbon film on lacey carbon supported film with 300-mesh gold, Ted Pella) were vacuum-heated at 150 °C overnight to remove any volatile hydrocarbons. A given catalyst was dispersed in ethanol and sonicated for 5 min, and the ethanol/powder

dispersion was droplet-deposited onto the grid. The grid was vacuum heated again at 150 °C overnight to remove the ethanol and hydrocarbons.

Bulk metal content of the catalysts was quantified using inductively coupled plasma optical emission spectroscopy (ICP-OES, Perkin Elmer Optima 8300) after aqua regia acid digestion of the materials.

XRD patterns were obtained by Rigaku Smartlab II instrument using Cu-Kα radiation in step size of 0.1° and speed at 10°/min, in the 2θ range of 30° to 55°. Crystal phase analysis was performed using the powder XRD analysis software (PDXL2) and mean grain size was obtained with the Scherrer equation.[62]

XPS data was collected by using a PHI Quantera SXM (ULVAC-PHI. Inc) with monochromatic Al Kα radiation (1486.7 eV). Samples were heat treated at 150 °C under H_2 for 1 h before the measurements of In 3d, Pd 3d, and Ni 2p core levels under UHV conditions. All the binding energy of each core-level electron was calibrated by the respective C 1s peak of graphitic carbon (284.5 eV).[63] CasaXPS software was used to fit the spectra and calculate surface metal compositions.

CO chemisorption was conducted with Micromeritics AutoChem II 2920. 50 mg of quartz wool was loaded into the U-shape glass tube, followed by loading 70 mg of catalyst. The sample was pretreated by reducing catalysts at 150 °C (10 °C/min ramp rate) under constant flow of 10% H_2/Ar (50 cm^3/min) for 1 h and switched the atmosphere to He under constant flow of 50 cm^3/min. The sample was then cooled down to 35 °C for CO chemisorption. Multiple pulses of CO (10% in He, 500 μL) was injected into the glass tube, and the amount of unabsorbed CO was monitored by the thermal conductivity detector (TCD) until a constant peak area was observed. The total amount of adsorbed CO quantified in this manner allows calculations of Pd dispersion.

The calculation for In deposited catalysts was done under the assumption that all of the metallic In and In_2O_3 has no effect on the CO chemisorption.[64] In addition, the calculation for Ni containing catalysts was conducted under the assumption that the exposed Ni surface had no influence on CO chemisorption. This assumption was made due to the relatively low

pretreatment temperature (150 °C) which was insufficient for the reduction of surface oxidized Ni that was formed during the synthesis.

The exposed Pd (E_{Pd}) and total Pd (T_{Pd}) values were calculated assuming a 1:1 CO:Pd stoichiometry[65,66] as follows:

$$\mathrm{E_{Pd},\mu mol/g_{cat}} = \frac{\mathrm{C_Q}}{22414} \times 10^6 \quad \text{Eq. 1}$$

$$\mathrm{T_{Pd},\mu mol/g_{cat}} = \frac{\mathrm{CW} \times (\mathrm{Pd,wt\%})}{106.42 \times \mathrm{CW}} \times 10^6 \quad \text{Eq. 2}$$

where C_Q is the total adsorbed CO (cm^3/g_{cat}-STP), 22414 is molar density of CO at STP (cm^3/mol), 10^6 is unit conversion from mol to μmol, CW is catalyst weight (g), Pd,wt% is wt% of Pd of catalyst, and 106.42 is the Pd atomic weight (g/mol).

The number of Pd binding site ($\#/g_{cat}$) was calculated using the exposed Pd (E_{Pd}):

$$\mathrm{Numbers\ of\ Pd\ binding\ site,\ \#/g_{cat}} = \mathrm{E_{Pd}} \times 10^{-6} \times \mathrm{N_A} \quad \text{Eq. 3}$$

where, 10^{-6} is unit conversion from μmol to mol and N_A is Avogadro's number (6.022×10^{23} mol^{-1}).

2.4. Catalyst Activity Characterization

Similar to our previous experiments,[36,67] catalytic reduction of NO_3^- experiments were conducted in a batch system at room temperature (23 °C). All experiments were conducted in a 120-mL screw-cap glass bottle with polytetrafluoroethylene (PTFE) threads and PTFE-silicone septum. All catalysts were heat treated at 150 °C under H_2 for 1 h before testing catalyst activity. Before taking out the catalysts after heat treatment, the samples were passivated under Ar for 15 min to prevent rapid oxidation of carbon. 50 mg of catalyst was added to 49.5 mL DIW and mixed slightly by hand (catalysts loading, g_{cat} = 1 g/L). The solution was then simultaneously bubbled with CO_2 and H_2 (both at 100 mL/min) for 15 min to maintain the solution to pH 4-6 and to use it as an electron donor, respectively, and to remove dissolved oxygen and fill the headspace with H_2 and CO_2 prior to introduction of NO_3^- stock solution. Subsequently, 0.5 mL of NO_3^- stock solution was injected into the sealed reactor to initiate the

200 catalytic reduction. The initial concentration of NO_3^- was 11.3 mg-N/L (50 mg-NO_3^-/L).

201 During the reaction, 1.5 mL aliquots were periodically extracted and immediately filtered
202 by 0.22 μm polyethersulfone syringe filter and analyzed the aliquots with ion-chromatography
203 (IC, Thermo Scientific Dionex Aquion IC System; Dionex Ionpac AS23&AG23 for NO_3^-/ NO_2^-
204 and CS12A&CG12A for ammonium, NH_4^+) for NO_3^-, NO_2^-, and NH_4^+. The limits of detection
205 for this method were 0.1 ppm NO_3^-, 0.1 ppm NO_2^-, and 0.1 ppm NH_4^+.

206 The reaction was carried out under mixing with a Teflon-coated magnetic stir bar at 600
207 rpm. We prepared two sets of each trimetallic InPdNi/AC and bimetallic InPd/AC catalysts and
208 ran the NO_3^- reduction reaction to check reproducibility.

209 The observed initial rate constant (k_{obs}, min^{-1}) was determined by assuming pseudo-first
210 order depending on the NO_3^- concentration within the first 15 min of reaction with the following
211 equation (Figure S1),

$$-\frac{dC_{NO_3^-}}{dt} = k_{obs} C_{NO_3^-} \quad \text{Eq. 4}$$

212 where, $C_{NO_3^-}$ and t is the concentration of NO_3^- and time, respectively. As NO_3^- reduction is
213 driven by the involvement of both exposed Pd and In, rather than Ni, the initial rate constant
214 was normalized to surface active metal concentration (determined from CO chemisorption
215 measurements of exposed Pd and from the assumption that all deposited In atoms are
216 exposed):

$$k_{cat} = \frac{k_{obs}}{[\{g_{cat}/L \times (Pd,wt\%) \times (E_{Pd}/T_{Pd})\} + \{g_{cat}/L \times (In,wt\%)\}]} \quad \text{Eq. 5}$$

217 where, Pd,wt% and In,wt% are wt% of Pd and In, respectively, and E_{Pd}/T_{Pd} is the fraction of
218 Pd atoms of a catalysts exposed to the surface. The denominator in the above equation (Eq.
219 5) represents the reactor content of surface active Pd and In (units of $g_{surface\text{-}Pd+In}L^{-1}$).

220 The by-product selectivity to NH_4^+ ($S_{NH_4^+}$) and NO_2^- ($S_{NO_2^-}$) were calculated using following
221 equations:

$$S_{NH_4^+} = \left(\frac{C_{NH_4^+}}{C_0 - C}\right) \times 100 \quad \text{Eq. 6}$$

$$S_{NO_2^-} = \left(\frac{C_{NO_2^-}}{C_0 - C}\right) \times 100 \quad \text{Eq. 7}$$

where, C_0, C, $C_{NH_4^+}$, and $C_{NO_2^-}$ are initial NO_3^- molar concentration, NO_3^- molar concentration at time t, NH_4^+ molar concentration at time t, and NO_2^- concentration at time t, respectively. As previous reports show only a trace amount of NO and N_2O is formed as an intermediate product, NO_2^- and NH_4^+ are the major reaction products from PdIn catalysts.[44,68] Therefore, we only considered NO_2^- and NH_4^+ for the selectivity.

2.5. DFT Computational Method

Periodic boundary condition DFT calculations were carried out as implemented in the Vienna ab-initio Simulation Package (VASP),[69] using the Perdew-Burke-Ernzerhof (PBE) functional in the framework of the Generalized Gradient Approximation (GGA).[70] Projector-augmented wave pseudopotentials explicitly include the Ni 3d and 4s, Pd 4d, and In 5s and 5p electrons.[71] The wavefunction was constructed from a summation of planewaves with energies up to 400 eV. There was less than a 0.01 eV difference in structure energies calculated at 500 eV as opposed to 400 eV, with no change in the attributed charge per atom.

The PdNi structure of PdNi/AC catalyst was chosen as a model to demonstrate the electron transfer effect. It was represented as a (111)-terminated slab model of Ni consisting of 7×7×4 Ni atoms, which was chosen as it is the lowest-energy surface termination.[72] The bottom two layers of Ni were considered fixed to their equilibrium lattice positions. Upon the Ni slab were placed two layers of Pd atoms in a triangular pyramidal shape, to represent the Pd island. The Brillouin zone was sampled with a 4×4×1 Γ-centered Monkhorst-Pack k-point mesh,[73] as there was less than 0.01 eV difference in structure energy when calculated with a 5×5×1 mesh. At least 18 Å of vacuum space was included in the direction perpendicular to the slab surface to minimize spurious self-interactions between the slab and its own periodic image. Additionally, dipole corrections to the slab were included in the Z-direction, in accordance with the method of Neugebauer *et al.*[74] Dispersion corrections were not included. Structure geometries were considered converged when forces on all the atoms were less than

0.01 eV/Å, and SCF convergence was reached when the energy changed by less than 1×10^{-5} eV. Total electronic charge on each atom was accounted for by the Bader charge method, as implemented by Tang *et al.*[75]

2.6. Cost Estimation of Catalysts

Instead of using only gram-scale metal prices, we estimated the catalyst cost that uses metal prices (from August 2024) extrapolated to kilogram amounts and the various costs associated with catalyst manufacture. We used a cost estimation software called CatCost™, for pre-commercial catalysts,[76] to consider a hypothetical purchase order of 907 kg (1 US ton) used in a continuously-stirred tank reactor (CSTR). This software provides a methodology to calculate cost based on standard manufacturing techniques scaled up from the synthesis procedures described for InPdNi/AC (Section 2.2.1-3), and for InPd1.3/AC (Section 2.2.4). Detailed information and calculations are provided in the Supporting Information S1.

3. Results and Discussion

3.1. Catalyst Compositions

We first determined the metal content of all synthesized catalysts via the ICP-OES elemental analysis (Table 1). Nearly all catalysts reached the target metal loadings within 10% error.

Table 1. Target and ICP-OES-measured metal catalyst compositions

Catalysts	Metal	Target (wt%)	Measured (wt%)	Atomic ratio In : Pd (at%)
InPd0.1Ni1.0/AC	In	0.05	0.052	38 : 62
	Pd	0.3	0.094	
	Ni	1.0	0.99	
InPd1.3/AC	In	0.05	0.044	3 : 97
	Pd	1.3	1.3	
InPd0.3/AC	In	0.05	0.045	12 : 88
	Pd	0.3	0.3	
InNi1.0/AC	In	0.05	0.051	
	Ni	1.0	0.98	
Pd0.1Ni1.0/AC	Pd	0.3	0.094	
	Ni	1.0	0.99	

Pd1.3/AC	Pd	1.3	1.3
Pd0.3/AC	Pd	0.3	0.3
Ni1.0/AC	Ni	1.0	1.0

The Pd content of the PdNi/AC and InPdNi/AC catalysts did not match the targeted wt% loading, with measured Pd loadings that were 3× lower than the targeted loadings. We repeated the PdNi/AC synthesis two more times and found the measured Pd loading to be consistent and to be 3× lower than the target Pd loading. The measured Pd loading for PdNi/AC is 0.094 (± 0.0006) wt%. We attribute this lower-than-expected Pd content to weak interaction between $PdCl_4^-$ species and the Ni surface during the synthesis procedure (Scheme 1), leading to detachment and loss of $PdCl_4^-$ species from Ni surface during the repeated washing process.

The measured Pd loading for the trimetallic InPdNi/AC catalyst showed similar Pd composition (0.093 wt%) to PdNi/AC catalyst, indicating the In deposition step did not change the Pd and Ni composition. For the sake of clarity, we use "Pd0.1Ni1.0/AC" and "InPd0.1Ni1.0/AC" terms to refer to these catalyst materials henceforth.

3.2. Catalytic Nitrate Reduction Behavior

Catalytic nitrate reduction occurred for materials containing both Pd and In (Figure 1), as expected.[36,37] Whereas the two bimetallic InPd compositions converted >96% of NO_3^- within 60 min (InPd1.3/AC) and >79% of NO_3^- within 120 min (InPd0.3/AC), trimetallic InPd0.1Ni1.0/AC was even more active.

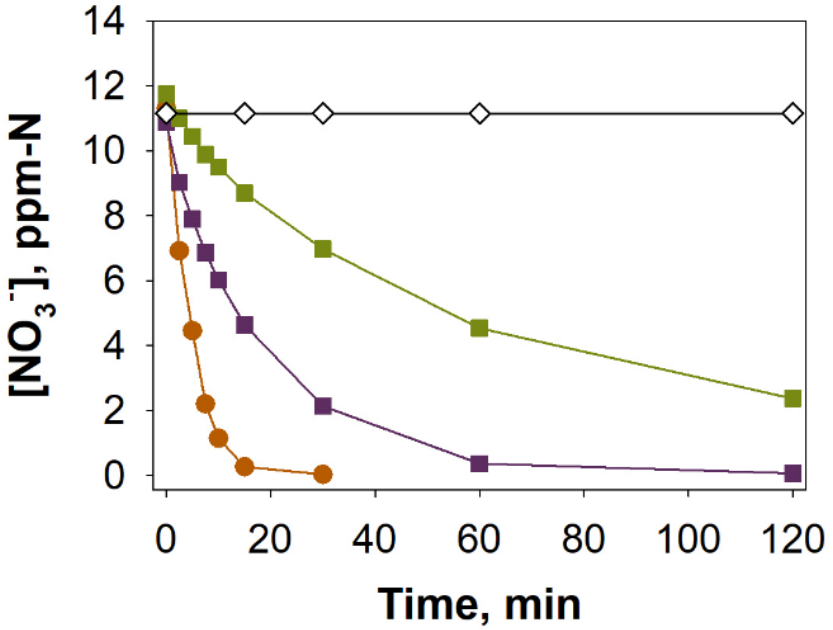

Figure 1. Concentration-time profiles of NO_3^- for InPd0.1Ni1.0/AC (●), InPd1.3/AC (■), InPd0.3/AC (■), and InNi1.0/AC (◇). Reaction conditions: 600 rpm stirring rate, 1 atm pressure (50/50 H_2/CO_2), pH ~ 4-6, temperature = 23 °C, catalyst charge = 1.0 g_{cat}/L (reactor content of surface active Pd and In = 0.7, 2.8, and 0.9 $mg_{surface\text{-}PdIn}$/L, respectively).

Its initial rate constant (k_{obs}) was ~4 and ~13 times larger than those for InPd1.3/AC and InPd0.3/AC, respectively. It converted >98% of NO_3^- within 15 min, even though the material contained less Pd (0.094 wt%, Table 1) and the reactor contained less total Pd (Table 2). To compare catalytic activity further, we calculated reaction rate constants normalized to the combined mass of Pd and In accessible to the reaction, as both metals participate in the nitrate reduction reaction. The fraction of Pd atoms of a catalysts exposed to the surface (E_{Pd}/T_{Pd}) was determined via CO chemisorption analysis and all In atoms were assumed to be exposed (the details of which are provided in Supporting Information S2 and Table S5).

The surface site normalized rate constant (k_{cat}) of InPd0.1Ni1.0/AC was higher than those of InPd1.3/AC and InPd0.3/AC, by ~18 and ~16 times, respectively. The catalytic reactions were carried twice; the concentration-time profiles confirmed data consistency. (Figure S4). Furthermore, InPd0.1Ni1.0/AC was compared to the previously reported InPd catalysts. The k_{cat} for InPd0.1Ni1.0/AC (349 $Lmin^{-1}g_{surface\ metal}^{-1}$) was 46 times higher than that

306 of 40 sc% In-on-Pd NPs (7.6 $Lmin^{-1}g_{surface\ metal}^{-1}$), as reported by Guo et al. (2018).[36]
307 Additionally, with respect to the initial rate constant normalized to the total Pd and In,
308 InPd0.1Ni1.0/AC (169 $Lmin^{-1}g_{total\ Pd+In}^{-1}$) was ~24 times higher than In-on-$Pd_{80}Au_{20}$ NPs (7
309 $Lmin^{-1}g_{total\ Pd+In}^{-1}$), as reported by Guo et al. (2022).[47]
310
311 Table 2. Comparison of catalytic nitrate reduction rate constants and metal content of reactor

Samples	**k_{obs} (10^{-2} min^{-1})**	**k_{cat} ($Lmin^{-1}g_{surface\ metal}^{-1}$)**	**Reactor Content of Surface Active Pd and In ($mg_{surface\text{-}Pd+In}L^{-1}$)**
InPd0.1Ni1.0/AC	24.7	349	0.7
InPd1.3/AC	5.6	19.9	2.8
InPd0.3/AC	1.9	22	0.9
InNi1.0/AC	0	0	Not applicable
Pd0.1Ni1.0/AC	0	0	Not applicable
Pd0.3/AC	0	0	Not applicable
Pd1.3/AC	0	0	Not applicable
Ni1.0/AC	0	0	Not applicable

312
313 The active catalysts generated both NO_2^- and NH_4^+ as reaction products (Figure 2). The
314 amount of generated NO_2^- increased rapidly in the first few minutes and then decreased
315 gradually over time (Figure 2a, inset).[29,36] NO_2^- selectivity decreased with NO_3^- conversion, as
316 the NO_2^- anions underwent reduction on the exposed Pd sites (Figure 2c).
317

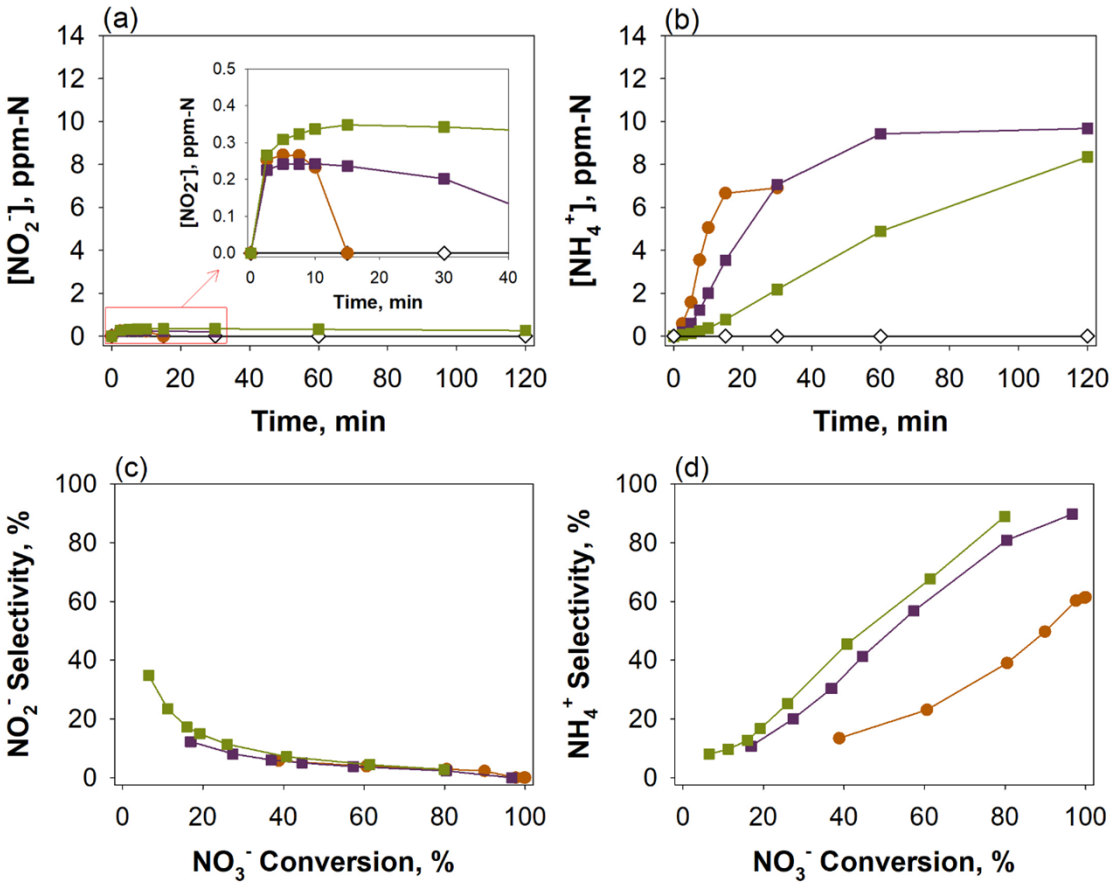

Figure 2. Concentration-time profiles of (a) NO_2^- and (b) NH_4^+ and (c,d) corresponding selectivity-conversion plots for InPd0.1Ni1.0/AC (●), InPd1.3/AC (■), InPd0.3/AC (■), and InNi1.0/AC (◇). Reaction conditions: 600 rpm stirring rate, 1 atm pressure (50/50 H_2/CO_2), pH ~ 4-6, temperature = 23 °C, catalyst charge = 1.0 g_{cat}/L.

NH_4^+ concentrations increased continuously with reaction time for the active catalysts (Figure 2b). At 50% conversion, NH_4^+ selectivity for InPd0.1Ni1.0/AC (18%) was 2.6× and 3× lower than those for InPd1.3/AC (48%) and InPd0.3/AC (55%) (Figure 2d). However, compared to the previously reported NH_4^+ selectivities for 40 sc% In-on-Pd NPs (<1.5%) and In-on-$Pd_{80}Au_{20}$ NPs (<5%),[36,47] the NH_4^+ selectivity for InPd0.1Ni1.0/AC is relatively high. Drinking water applications favor as low ammonium by-product as possible, and production of N_2 is preferred. We note these NH_4^+ selectivity values are higher compared to the unsupported In-on-Pd NPs from our previous work (~5%),[36] which we attribute to catalyst support effects. OH^- anions form as NO_3^- and NO_2^- anions reduce on the metal surface, but their diffusion into the bulk solution is constrained by the small AC pores, leading to localized higher pH within

the pores.[77,78] As reported in literature, high pH values favor the formation of NH_4^+ over N_2.[79–81] Thus, our use of AC likely resulted in the buildup of basicity within its pores during the catalytic reaction, generating more NH_4^+ compared to catalysts on larger-pore supports (*e.g.*, porous alumina oxides) and other unsupported catalysts.[77,78,82,83]

3.3. Metal Structure of the Trimetallic Catalyst

To elucidate the origin of the enhanced NO_3^- reduction performance of InPd0.1Ni1.0/AC, we examined the metal distribution of InPd0.1Ni1.0/AC via HAADF-STEM (Figure 3). Ni particles are located on the AC surface, which are ~16 nm in size, similar to the XRD-derived grain size (Table S6). Pd domains were found primarily on the Ni particle surface, and were ~3-5 nm in size; Pd was not detected through XRD (Figure S5), due to the low Pd content and too-small-to-detect grains.

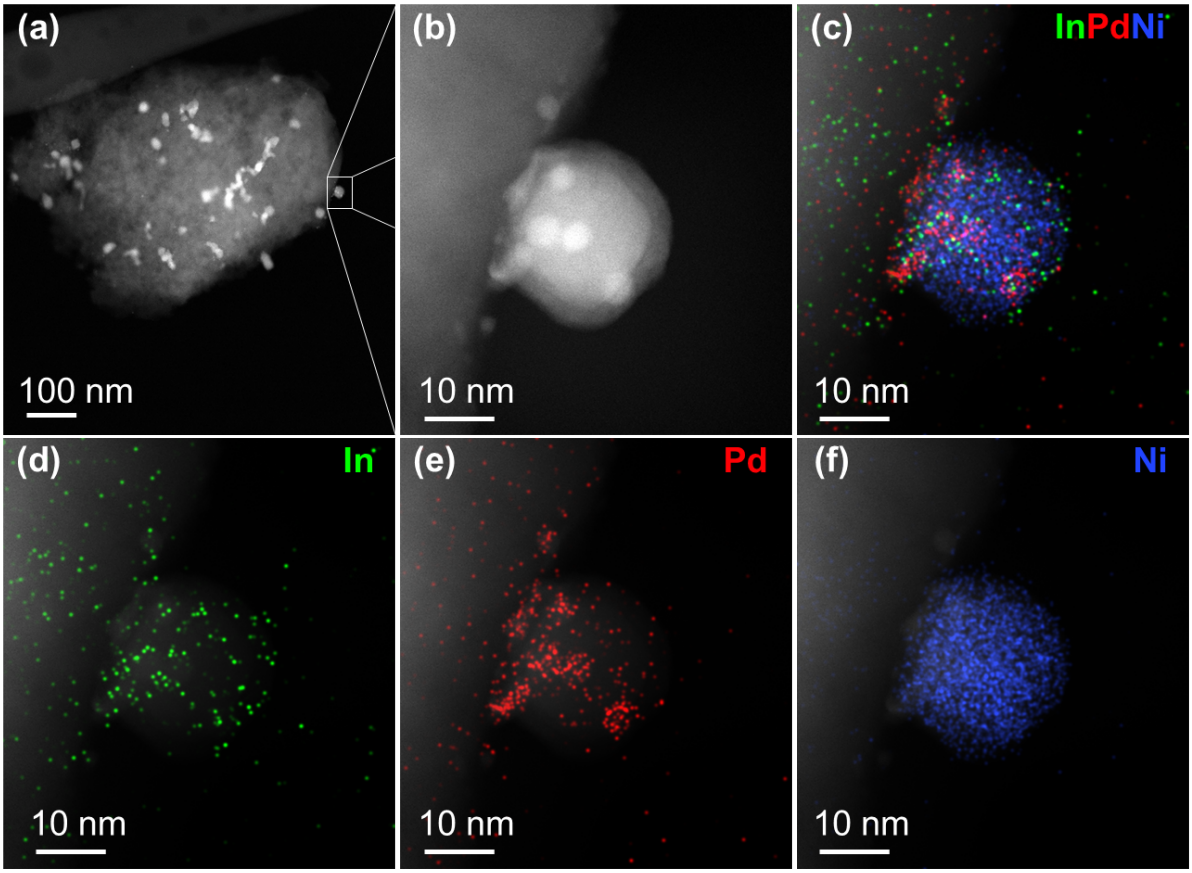

Figure 3. (a) A representative HAADF-STEM, (b) a higher-magnification, and (c) a composite elemental map image of the trimetallic InPd0.1Ni1.0/AC. (d-f) Energy-dispersive x-ray spectroscopy (EDX) individual maps of (d) In, (e) Pd, and (f) Ni elements.

In atoms are located mostly near the Pd atoms. Knowing that the number of Pd binding sites is lower after In deposition on Pd0.1Ni1.0/AC and the number of Pd binding site covered by In is similar across the In-containing catalysts (Table S5), we conclude that In atoms are situated on top of Pd, and that InPd0.1Ni1.0/AC essentially has an "In-on-Pd-on-Ni" metal arrangement.

XPS analysis of the trimetallic and bimetallic compositions provided information about Pd, In, and Ni oxidation states within the x-ray penetration depth (<10 nm) of the material (Figure 4). For Pd 3d core level (Figure 4a), an asymmetric Pd^0 $3d_{5/2}$ peak at 335.3 eV (InPd0.1Ni1.0/AC and Pd0.1Ni1.0/AC) or 335.5 eV (InPd1.3/AC, Pd1.3/AC, InPd0.3/AC, and Pd0.3/AC) was coupled with the respective Pd^0 $3d_{3/2}$ peak (located 5.3 eV higher due to the spin-orbital splitting).[84,85]

For the In 3d peak observed in the catalysts (Figure 4b), both the asymmetric metallic In^0 and symmetric oxidized In^{3+} were observed: In^0 $3d_{5/2}$ (In^{3+} $3d_{5/2}$) peak at 443.8 eV (444.7 eV, In_2O_3) for InPd0.1Ni1.0/AC; 443.8 eV (445.2 eV, $In(OH)_3$) for InPd1.3/AC; and 443.7 eV (445.1 eV, $In(OH)_3$) for InPd0.3/AC, coupled with their respective In $3d_{3/2}$ peaks located 7.6 eV higher.[86,87] As expected, oxidized In was observed for both the trimetallic and bimetallic compositions, which is due to the facile oxidation of In when exposed to air.[88]

Ni1.0/AC and InNi1.0/AC showed corresponding peaks of Ni^0, NiO, and $Ni(OH)_2$ at 852.6, 855.0, and 856.9 eV, respectively, while bimetallic Pd0.1Ni1.0/AC and trimetallic InPd0.1Ni1.0/AC showed peaks at 853.2, 855.9, and 857.3 eV, respectively.[89]

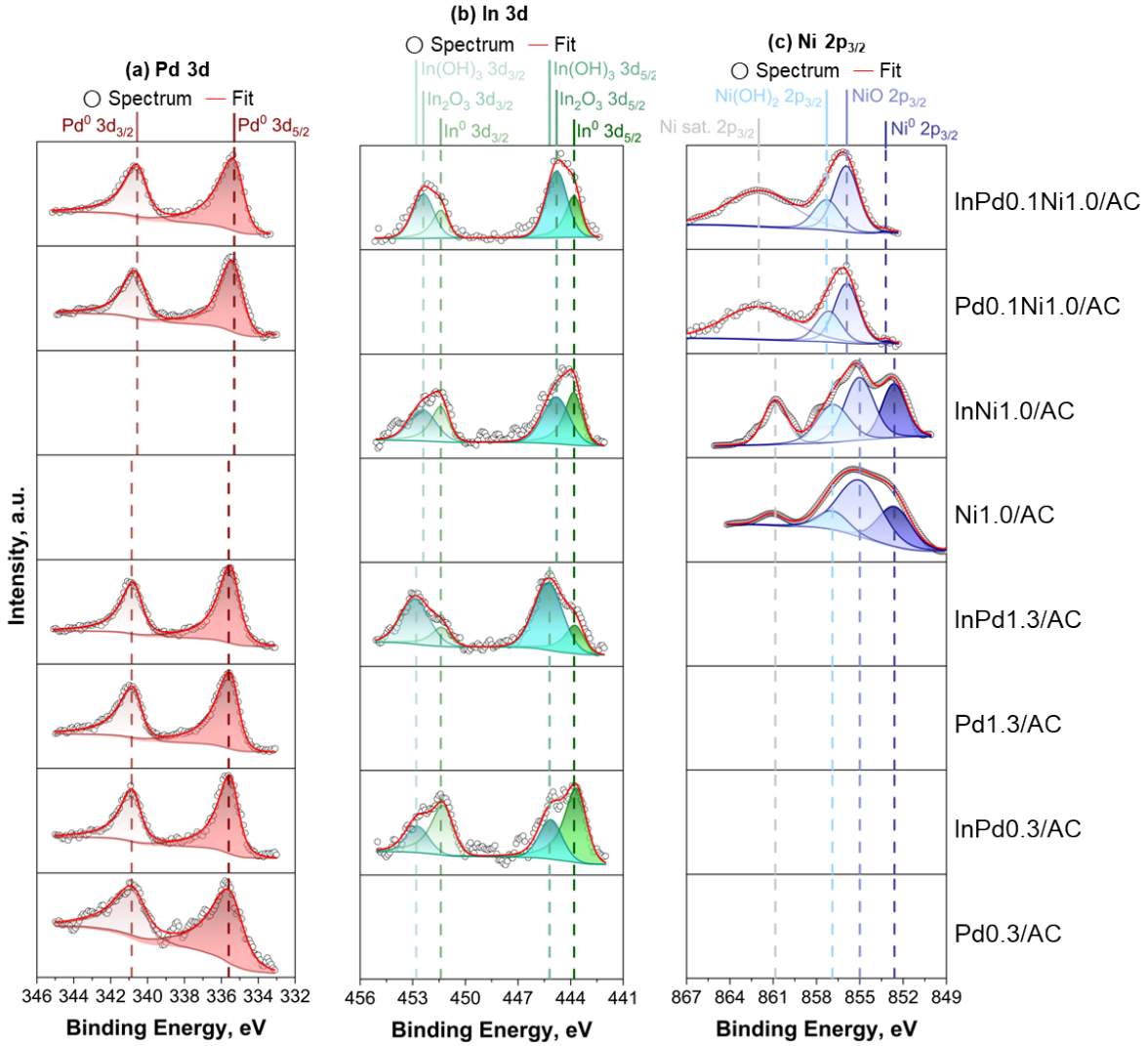

Figure 4. XPS spectra at the (a) Pd 3d, (b) In 3d, and (c) Ni $2p_{3/2}$ core levels of trimetallic, bimetallic, and monometallic compositions.

With the bimetallic catalysts (InPd0.3/AC and InPd1.3/AC), we observed no difference in the Pd 3d binding energies nor in the In 3d binding energies, both matching well with those reported for Pd 3d and In 3d. This indicates insufficient electronic interaction between In and Pd at their interface to alter their binding energies.

However, the Pd^0 $3d_{5/2}$ binding energy of the trimetallic InPd0.1Ni1.0/AC (335.3 eV) shifted to a lower binding energy (by 0.2 eV) compared to the InPd and Pd catalysts. The Ni in trimetallic catalyst showed a positive shift of 0.6 eV compared to the monometallic Ni1.0/AC,

while no peak shift is observed for In; the same can be observed in Pd0.1Ni1.0/AC catalyst. The observed peak shift in both Pd and Ni indicates that Pd has a higher electron density and Ni has a lower electron density. Overall, the electron transfer (from Ni to Pd) leads to a change in the surface electronic structure of both metals, driven by their electronegativity difference.[54]

To corroborate the Pd-Ni metal electronic interactions, DFT calculations were performed. Figure 5 shows the difference in electron density Δe ($|e^-|$) of the bimetallic catalyst at the junction between Ni and Pd atoms. The Ni atoms at the center of the junction (Figure 5a) were depleted of roughly 0.1 electrons per atom, while the Ni atoms around the base of the Pd island had smaller (~0.02 electrons) charge deviations. The bottom layer of Pd atoms (Figure S7) localized much of the transferred charge, particularly around the perimeter of the island, where the charge surplus was ~0.1 electrons per atom. The three Pd atoms at the center of the base layer (Figure S7), as well as the Pd atoms comprising the top layer of the island (Figure 5b), localized a smaller portion of the charge transferred, roughly ~ 0.02-0.05 electrons per atom. DFT results show electron donation from the Ni atoms to the Pd atoms (as evidenced by the mean Δe values).

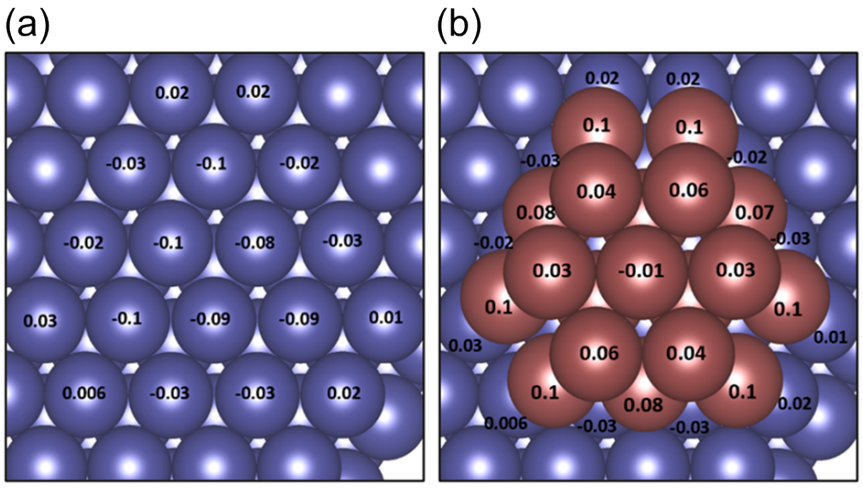

Figure 5. Δe values ($|e^-|$) of Pd or In atoms according to Bader charge analysis of PdNi structure modeled as a Ni slab (blue-colored atoms) supporting a three-dimensional ensemble of Pd atoms (red-colored atoms) shown in (b) and not in (a). Blue: Ni atoms, Red: Pd atoms).

3.4. Mechanistic Explanation of Enhanced Nitrate Reduction for the Trimetallic Catalyst

The widely accepted mechanism governing NO_3^- reduction by InPd catalysts involves two distinct active sites, In and Pd. The step that limits the reaction rate is facilitated by metallic In, which adsorbs NO_3^- ($NO_{3(ads)}^-$) and reduces it to NO_2^- ($NO_{2(ads)}^-$). Then the Pd sites play a dual role in the subsequent process: first, they reduce $NO_{2(ads)}^-$ to eventually form N_2 and/or NH_4^+; and second, they generate hydrogen adatoms from H_2 necessary to reduce the oxidized In, regenerating the metallic In.[38]

We propose a similar mechanism for the trimetallic catalyst, in which the Ni itself does not participate in any of these surface reaction steps but it affects the reaction through the earlier-discussed electronic effects. The initial step involves the reduction of $NO_{3(ads)}^-$ on In sites to form $NO_{2(ads)}^-$, followed by the migration of $NO_{2(ads)}^-$ to a Pd site or its desorption from the In site into the bulk solution ($NO_{2(aq)}^-$). When the $NO_{2(ads)}^-$ on Pd site remains isolated from other N-species (intermediate daughter species of NO_2^-, such as $NO_{(ads)}$ and $N_{(ads)}$, or $NO_{2(aq)}^-$), the favored outcome is the formation of NH_4^+. However, if additional surface N-species are present at neighboring Pd sites, N_2 formation favors via the coupling amongst N-species and/or the reaction of $NO_{(ads)}$ with $NO_{2(aq)}^-$ in an Eley-Rideal-like mechanism.[68,90,91]

Rapid reduction of NO_3^- to NO_2^- can be correlated to the electron transfer from Ni to Pd, similar to mechanisms proposed for other hydrogenation reactions.[54,92] We suggest the electron-rich Pd atoms (adjacent to Ni atoms) promotes the reduction of NO_3^- and the regeneration of oxidized In, accelerating the reduction kinetics of NO_3^-. Likewise, NO_2^- undergoes rapid reduction on the Pd sites (Figure S6), aligning with the understanding that electron rich Pd enhances the NO_2^- reduction reaction.[93] The enhanced reduction of NO_3^- to NO_2^- on In surface and NO_2^- to NO on Pd surface results in a higher surface coverage of N-species on Pd, thereby promoting the possibility of coupling of N-species that leads to the formation of more N_2. This notion is consistent with the observed lower ammonium selectivity for InPd0.1Ni1.0/AC (18% at 50% nitrate conversion), compared to those for the bimetallics (48% and 55%, Section 3.2).

3.5. Catalyst Cost Estimation Based on Precursors and Large-Scale Manufacturing

The simplest and most common method to estimate catalyst cost is to perform a weighted average (using the percentile composition) of each component multiplied by the spot price of the metals and support (Table S1). This approach projects the cost of InPd1.3/AC and InPd0.1Ni1.0/AC to be $391/kg and $30/kg, respectively (Table S2). The trimetallic cost is >12× lower, but these values do not reflect manufacturing costs and do not use metal precursor cost.

The CatCost estimation software offers a solution for approximating the expenses associated with producing catalysts in the pre-commercial stage. It leverages well-accepted methods and industry-standard resources to give useful insights throughout the various phases of catalyst research and development (Scheme S1),[61] accounting for the extrapolated cost of precursor salts, materials, and processing steps. This approach projects “catalyst purchase cost” for InPd1.3/AC and InPd0.1Ni1.0/AC to be $1388 and $190 per kg of catalyst, respectively (Table S3). This more realistic estimation indicates the trimetallic catalyst purchase cost is 86% lower than that of the bimetallic catalyst.

An improved comparison of catalyst purchase cost should also consider the value of the catalyst at the *end* of its useful life. In this regard, the CatCost estimation software further evaluates the “spent catalyst value” by assessing three distinct options for spent catalyst: i) metals recovery, ii) sale, and iii) landfill. The software evaluates the value of each option and automatically chooses the most appropriate one. For both catalysts, the most favorable option was metals recovery since the recoverable Pd value ($26.45/kg for trimetallic and $368.43/kg for bimetallic catalyst) is much higher than the other two options (Figure S12a and S13a). Considering expenses for the total recovery fees related to the metal recovery ($6.85/kg for the trimetallic and $12.07/kg for the bimetallic), the spent catalyst value for InPd0.1Ni1.0/AC catalysts ($19.6/kg) was ~18× lower compared to InPd1.3/AC ($356.35/kg). Overall, the “net catalyst cost” for InPd1.3/AC and InPd0.1Ni1.0/AC was calculated respectively as $1028 and $170 per kg of catalyst (83% less).

3.6. Hypothetical Catalytic Reactor Performance Comparison

To illustrate the benefits of the improved nitrate reduction catalyst in a different manner, we estimated the treatment effectiveness of the two catalysts used in a CSTR (*e.g.*, a Berty-type configuration in which the catalyst material does not exit the effluent). We considered the simple scenario in which the CSTR (charged with either catalyst at 1 kg per 1000 L reactor volume) treats an influent nitrate concentration of 50 mg-N/L, such that the effluent concentration is 10 mg-N/L. To reach this 80% nitrate conversion, the required hydraulic residence time (τ) is ~16 and ~71 min, respectively, for InPd0.1Ni1.0/AC and InPd1.3/AC. The trimetallic catalyst-containing CSTR is thus ~4.4× effective, *i.e.*, 4.4× more water can be treated (Supporting Information S1.1). If the less effective bimetallic catalyst is substituted into the trimetallic catalyst-containing CSTR (operating at τ = ~16 min), the resulting reactor would not reach 80% nitrate conversion (~48%) and would not satisfy the 10 mg-N/L effluent target concentration (~26 mg-N/L). These calculations indicate a substantial gain in nitrate treatment performance resulting from the incorporation of Ni into the InPd catalyst.

The trimetallic catalyst ($170/kg) costs six times less the bimetallic ($1028/kg), and so we contend that it is ~26 times less expensive to use the trimetallic for the same treatment capacity. Further work is needed to design a Pd-based catalytic destruction treatment system and to evaluate its commercial viability against current available technologies through technoeconomic analysis. We expect that water matrix effects will lower catalyst activity but it is not yet known to what extent. Catalytic materials stability considerations require quantitative assessment of any potential leaching that may lead to metal loss, catalyst attrition, and long-term treatment performance degradation. And, the trimetallic catalyst would require further improvement with regard to nitrate reduction selectivity; ideally, ammonium should not be formed.

4. Conclusion

We designed and synthesized a trimetallic catalyst active for nitrate reduction. Showcasing the benefits of the incorporated Ni metal, catalytic activity and N_2 selectivity of the trimetallic composition were significantly greater compared to bimetallic InPd. HAADF-STEM analysis showed the In-on-Pd-on-Ni metal nanostructure supported on activated carbon, which reflected the sequential nature of the synthesis procedure. XPS and DFT calculations revealed electron transfer from Ni to Pd, rendering Pd electronically rich and more catalytically active. Metal precursor cost, manufacturing cost at the multi-kg scale, and spent metal recovery value are more appropriate parameters than metal spot prices for realistic catalyst cost estimation. Ni incorporation lowered the net catalyst cost by 83% according to a CatCost analysis, such that the trimetallic composition was six times less expensive than the bimetallic composition. Using a simple continuously-stirred tank reactor model, we estimated the trimetallic catalyst improves treatment effectiveness by >4 times and lowers the catalyst cost by 26 times to achieve the same treatment capacity as for the bimetallic catalyst. This study demonstrates and explains the catalytic performance improvements of Ni incorporation into the InPd nitrate reduction catalyst, which should be advantageous for other clean-water reactions.

5. Associated Content

Supporting Information

Detailed cost estimation of catalysts; CO chemisorption, BET surface area, XRD, and XPS analysis; bulk-scale cost extrapolation; duplicated reaction results; NO_2^- reaction result; Bader charge analysis of PdNi; Step method synthesis process of catalysts; and CatCost estimation results

6. Author Information

Corresponding Author

Michael S. Wong - Department– of Civil and Environmental Engineering, Rice University, 6100 Mainstreet, Houston, TX 77005, USA, Nanosystems Engineering Research Center for

Nanotechnology-Enabled Water Treatment, 6100 Mainstreet, Houston, TX 77005, USA, Department of Chemical and Biomolecular Engineering, Rice University, 6100 Mainstreet, Houston, TX 77005, USA, Department of Materials Science and NanoEngineering, 6100 Mainstreet, Houston, TX 77005, USA, Department of Chemistry, Rice University, 6100 Mainstreet, Houston, TX 77005, USA, Rice Water Institute, Rice University, Houston, TX 77005, USA, Rice Advanced Materials Institute, Rice University, Houston, TX 77005, USA

7. Author Contributions

Kiheon Hong Investigation leader, conceptualization, data curation, formal analysis, writing – original draft; **Daniel J. Rivera** investigation, visualization, writing – review & editing; **Juan A. Donoso** investigation, visualization, writing – review & editing; **Bongki Shin** investigation, visualization; **Hunter P. Jacobs** review & editing; **Byeong Jun Cha** review & editing; **Kimberly N. Heck** review & editing; **Welman C. Elias** review & editing; **Paul Westerhoff** project administration, review & editing; **Yimo Han** resources, review & editing; **Christopher L. Muhich** resources, review & editing; **Michael S. Wong** conceptualization, funding acquisition, supervision, project administration, writing – review & editing

8. Notes

The authors declare no competing financial interest.

9. Acknowledgments

This work was supported by the National Science Foundation (NSF) through the Nanosystems Engineering Research Center for Nanotechnology-Enabled Water Treatment under project EEC-1449500. The authors thank the Rice University Shared Equipment Authority (SEA) for use of the XRD, XPS, ICP-OES, and BET equipment, and IMRA America, Inc. for additional funding support.

10. References

(1) Spalding, R. F.; Exner, M. E. Occurrence of Nitrate in Groundwater—A Review. J. Environ. Qual. 1993, 22 (3), 392–402. https://doi.org/10.2134/jeq1993.00472425002200030002x.

(2) Ahmed, M.; Rauf, M.; Mukhtar, Z.; Saeed, N. A. Excessive Use of Nitrogenous Fertilizers: An Unawareness Causing Serious Threats to Environment and Human Health. Environ. Sci. Pollut. Res. 2017, 24 (35), 26983–26987. https://doi.org/10.1007/s11356-017-0589-7.

(3) Environmental Protection Agency. Edition of the Drinking Water Standards and Health Advisories, Fed. Regist. 2002, EPA-822-R-02-038.

(4) Gulis, G.; Czompolyova, M.; Cerhan, J. R. An Ecologic Study of Nitrate in Municipal Drinking Water and Cancer Incidence in Trnava District, Slovakia. Environ. Res. 2002, 88 (3), 182–187. https://doi.org/10.1006/enrs.2002.4331.

(5) Rogan, W. J.; Brady, M. T.; the Committee on Environmental Health, and the Committee on Infectious Diseases. Drinking Water From Private Wells and Risks to Children. Pediatrics 2009, 123 (6), e1123–e1137. https://doi.org/10.1542/peds.2009-0752.

(6) Weyer, P. J.; Cerhan, J. R.; Kross, B. C.; Hallberg, G. R.; Kantamneni, J.; Breuer, G.; Jones, M. P.; Zheng, W.; Lynch, C. F. Municipal Drinking Water Nitrate Level and Cancer Risk in Older Women: The Iowa Women's Health Study: Epidemiology 2001, 12 (3), 327–338. https://doi.org/10.1097/00001648-200105000-00013.

(7) Cliford, D.; Liu, X. Ion Exchange for Nitrate Removal. J. - Am. Water Works Assoc. 1993, 85 (4), 135–143. https://doi.org/10.1002/j.1551-8833.1993.tb05971.x.

(8) Samatya, S.; Kabay, N.; Yüksel, Ü.; Arda, M.; Yüksel, M. Removal of Nitrate from Aqueous Solution by Nitrate Selective Ion Exchange Resins. React. Funct. Polym. 2006, 66 (11), 1206–1214. https://doi.org/10.1016/j.reactfunctpolym.2006.03.009.

(9) Kapoor, A.; Viraraghavan, T. Nitrate Removal From Drinking Water—Review. J. Environ. Eng. 1997, 123 (4), 371–380. https://doi.org/10.1061/(ASCE)0733-9372(1997)123:4(371).

(10) Schoeman, J. J.; Steyn, A. Nitrate Removal with Reverse Osmosis in a Rural Area in South Africa. Desalination 2003, 155 (1), 15–26. https://doi.org/10.1016/S0011-9164(03)00235-2.

(11) El Midaoui, A.; Elhannouni, F.; Taky, M.; Chay, L.; Menkouchi Sahli, M. A.; Echihabi, L.; Hafsi, M. Optimization of Nitrate Removal Operation from Ground Water by Electrodialysis. Sep. Purif. Technol. 2002, 29 (3), 235–244. https://doi.org/10.1016/S1383-5866(02)00092-8.

(12) Hell, F.; Lahnsteiner, J.; Frischherz, H.; Baumgartner, G. Experience with Full-Scale Electrodialysis for Nitrate and Hardness Removal. Desalination 1998, 117 (1), 173–180. https://doi.org/10.1016/S0011-9164(98)00088-5.

(13) Yang, T.; Doudrick, K.; Westerhoff, P. Photocatalytic Reduction of Nitrate Using Titanium Dioxide for Regeneration of Ion Exchange Brine. Water Res. 2013, 47 (3), 1299–1307. https://doi.org/10.1016/j.watres.2012.11.047.

(14) Lehman, S. G.; Badruzzaman, M.; Adham, S.; Roberts, D. J.; Clifford, D. A. Perchlorate

and Nitrate Treatment by Ion Exchange Integrated with Biological Brine Treatment. Water Res. 2008, 42 (4–5), 969–976. https://doi.org/10.1016/j.watres.2007.09.011.

(15) van der Hoek, J. P.; van der Ven, P. J. M.; Klapwijk, A. Combined Ion Exchange/Biological Denitrification for Nitrate Removal from Ground Water under Different Process Conditions. Water Res. 1988, 22 (6), 679–684. https://doi.org/10.1016/0043-1354(88)90178-9.

(16) Richard, Y.; Thebault, P. Biological Removal of Nitrates-Report on 7 Years of Operation and Progress. Water Supply 1992, 10 (3), 151–160.

(17) van de Graaf, A. A.; Mulder, A.; Slijkhuis, H.; Robertson, L. A.; Kuenen, J. G. Anoxic Ammonium Oxidation. Proc. Fifth Eur. Congr. Biotechnol. 1990, 1, 338–391.

(18) Ziv-El, M. C.; Rittmann, B. E. Systematic Evaluation of Nitrate and Perchlorate Bioreduction Kinetics in Groundwater Using a Hydrogen-Based Membrane Biofilm Reactor. Water Res. 2009, 43 (1), 173–181. https://doi.org/10.1016/j.watres.2008.09.035.

(19) Hu, Q.; Westerhoff, P.; Vermaas, W. Removal of Nitrate from Groundwater by Cyanobacteria: Quantitative Assessment of Factors Influencing Nitrate Uptake. Appl. Environ. Microbiol. 2000, 66 (1), 133–139. https://doi.org/10.1128/AEM.66.1.133-139.2000.

(20) Garcia-Segura, S.; Lanzarini-Lopes, M.; Hristovski, K.; Westerhoff, P. Electrocatalytic Reduction of Nitrate: Fundamentals to Full-Scale Water Treatment Applications. Appl. Catal. B Environ. 2018, 236, 546–568. https://doi.org/10.1016/j.apcatb.2018.05.041.

(21) Xu, H.; Ma, Y.; Chen, J.; Zhang, W.; Yang, J. Electrocatalytic Reduction of Nitrate – a Step towards a Sustainable Nitrogen Cycle. Chem. Soc. Rev. 2022, 51 (7), 2710–2758. https://doi.org/10.1039/D1CS00857A.

(22) Werth, C. J.; Yan, C.; Troutman, J. P. Factors Impeding Replacement of Ion Exchange with (Electro)Catalytic Treatment for Nitrate Removal from Drinking Water. ACS EST Eng. 2021, 1 (1), 6–20. https://doi.org/10.1021/acsestengg.0c00076.

(23) Hua, Y.; Song, N.; Wu, Z.; Lan, Y.; Luo, H.; Song, Q.; Yang, J. Cu–Fe Synergistic Active Sites Boost Kinetics of Electrochemical Nitrate Reduction. Adv. Funct. Mater. 2024, 34 (21), 2314461. https://doi.org/10.1002/adfm.202314461.

(24) Wu, Z.; Song, Y.; Guo, H.; Xie, F.; Cong, Y.; Kuang, M.; Yang, J. Tandem Catalysis in Electrocatalytic Nitrate Reduction: Unlocking Efficiency and Mechanism. Interdiscip. Mater. 2024, 3 (2), 245–269. https://doi.org/10.1002/idm2.12152.

(25) Luo, H.; Li, S.; Wu, Z.; Jiang, M.; Kuang, M.; Liu, Y.; Luo, W.; Zhang, D.; Yang, J. Relay Catalysis of Fe and Co with Multi-Active Sites for Specialized Division of Labor in Electrocatalytic Nitrate Reduction Reaction. Adv. Funct. Mater. 2024, 2403838. https://doi.org/10.1002/adfm.202403838.

(26) Martínez, J.; Ortiz, A.; Ortiz, I. State-of-the-Art and Perspectives of the Catalytic and Electrocatalytic Reduction of Aqueous Nitrates. Appl. Catal. B Environ. 2017, 207, 42–59. https://doi.org/10.1016/j.apcatb.2017.02.016.

(27) Teng, W.; Bai, N.; Liu, Y.; Liu, Y.; Fan, J.; Zhang, W. Selective Nitrate Reduction to Dinitrogen by Electrocatalysis on Nanoscale Iron Encapsulated in Mesoporous Carbon.

Environ. Sci. Technol. 2018, 52 (1), 230–236. https://doi.org/10.1021/acs.est.7b04775.

(28) Vorlop, K.-D.; Tacke, T. Erste Schritte auf dem Weg zur edelmetallkatalysierten Nitrat- und Nitrit-Entfernung aus Trinkwasser. Chem. Ing. Tech. 1989, 61 (10), 836–837. https://doi.org/10.1002/cite.330611023.

(29) Prüsse, U.; Vorlop, K.-D. Supported Bimetallic Palladium Catalysts for Water-Phase Nitrate Reduction. J. Mol. Catal. Chem. 2001, 173 (1–2), 313–328. https://doi.org/10.1016/S1381-1169(01)00156-X.

(30) Lemaignen, L.; Tong, C.; Begon, V.; Burch, R.; Chadwick, D. Catalytic Denitrification of Water with Palladium-Based Catalysts Supported on Activated Carbons. Catal. Today 2002, 75 (1–4), 43–48. https://doi.org/10.1016/S0920-5861(02)00042-1.

(31) Choe, J. K.; Bergquist, A. M.; Jeong, S.; Guest, J. S.; Werth, C. J.; Strathmann, T. J. Performance and Life Cycle Environmental Benefits of Recycling Spent Ion Exchange Brines by Catalytic Treatment of Nitrate. Water Res. 2015, 80, 267–280. https://doi.org/10.1016/j.watres.2015.05.007.

(32) Strukul, G.; Gavagnin, R.; Pinna, F.; Modaferri, E.; Perathoner, S.; Centi, G.; Marella, M.; Tomaselli, M. Use of Palladium Based Catalysts in the Hydrogenation of Nitrates in Drinking Water: From Powders to Membranes. Catal. Today 2000, 55 (1–2), 139–149. https://doi.org/10.1016/S0920-5861(99)00233-3.

(33) Ilinitch, O. M.; Cuperus, F. P.; Nosova, L. V.; Gribov, E. N. Catalytic Membrane in Reduction of Aqueous Nitrates: Operational Principles and Catalytic Performance. Catal. Today 2000, 56 (1–3), 137–145. https://doi.org/10.1016/S0920-5861(99)00270-9.

(34) Bell, A. T. The Impact of Nanoscience on Heterogeneous Catalysis. Science 2003, 299 (5613), 1688–1691. https://doi.org/10.1126/science.1083671.

(35) Zaera, F. Nanostructured Materials for Applications in Heterogeneous Catalysis. Chem Soc Rev 2013, 42 (7), 2746–2762. https://doi.org/10.1039/C2CS35261C.

(36) Guo, S.; Heck, K.; Kasiraju, S.; Qian, H.; Zhao, Z.; Grabow, L. C.; Miller, J. T.; Wong, M. S. Insights into Nitrate Reduction over Indium-Decorated Palladium Nanoparticle Catalysts. ACS Catal. 2018, 8 (1), 503–515. https://doi.org/10.1021/acscatal.7b01371.

(37) Elias, W. C.; Heck, K. N.; Guo, S.; Yazdi, S.; Ayala-Orozco, C.; Grossweiler, S.; Domingos, J. B.; Ringe, E.; Wong, M. S. Indium-Decorated Pd Nanocubes Degrade Nitrate Anions Rapidly. Appl. Catal. B Environ. 2020, 276, 119048. https://doi.org/10.1016/j.apcatb.2020.119048.

(38) Yin, Y. B.; Guo, S.; Heck, K. N.; Clark, C. A.; Conrad, C. L.; Wong, M. S. Treating Water by Degrading Oxyanions Using Metallic Nanostructures. ACS Sustain. Chem. Eng. 2018, 6 (9), 11160–11175. https://doi.org/10.1021/acssuschemeng.8b02070.

(39) Qian, H.; Zhao, Z.; Velazquez, J. C.; Pretzer, L. A.; Heck, K. N.; Wong, M. S. Supporting Palladium Metal on Gold Nanoparticles Improves Its Catalysis for Nitrite Reduction. Nanoscale 2014, 6 (1), 358–364. https://doi.org/10.1039/C3NR04540D.

(40) Vorlop, K.-D.; Hörold, S.; Pohlandt, K. Optimierung von Trägerkatalysatoren Zur Selektiven Nitritentfernung Aus Wasser. Chem. Ing. Tech. 1992, 64 (1), 82–83. https://doi.org/10.1002/cite.330640119.

(41) Hörold, S.; Vorlop, K.-D.; Tacke, T.; Sell, M. Development of Catalysts for a Selective

Nitrate and Nitrite Removal from Drinking Water. Catal. Today 1993, 17 (1), 21–30. https://doi.org/10.1016/0920-5861(93)80004-K.

(42) Prüsse, U.; Hörold, S.; Vorlop, K.-D. Einfluß Der Präparationsbedingungen Auf Die Eigenschaften von Bimetallkatalysatoren Zur Nitratentfernung Aus Wasser. Chem. Ing. Tech. 1997, 69 (1–2), 93–97. https://doi.org/10.1002/cite.330690114.

(43) Prüsse, U.; Hähnlein, M.; Daum, J.; Vorlop, K.-D. Improving the Catalytic Nitrate Reduction. Catal. Today 2000, 55 (1), 79–90. https://doi.org/10.1016/S0920-5861(99)00228-X.

(44) Chaplin, B. P.; Shapley, J. R.; Werth, C. J. The Selectivity and Sustainability of a Pd–In/γ-Al2O3 Catalyst in a Packed-Bed Reactor: The Effect of Solution Composition. Catal. Lett. 2009, 130 (1), 56–62. https://doi.org/10.1007/s10562-009-9883-4.

(45) Chaplin, B. P.; Roundy, E.; Guy, K. A.; Shapley, J. R.; Werth, C. J. Effects of Natural Water Ions and Humic Acid on Catalytic Nitrate Reduction Kinetics Using an Alumina Supported Pd−Cu Catalyst. Environ. Sci. Technol. 2006, 40 (9), 3075–3081. https://doi.org/10.1021/es0525298.

(46) Chaplin, B. P.; Shapley, J. R.; Werth, C. J. Regeneration of Sulfur-Fouled Bimetallic Pd-Based Catalysts. Environ. Sci. Technol. 2007, 41 (15), 5491–5497. https://doi.org/10.1021/es0704333.

(47) Guo, S.; Li, H.; Heck, K. N.; Luan, X.; Guo, W.; Henkelman, G.; Wong, M. S. Gold Boosts Nitrate Reduction and Deactivation Resistance to Indium-Promoted Palladium Catalysts. Appl. Catal. B Environ. 2022, 305, 121048. https://doi.org/10.1016/j.apcatb.2021.121048.

(48) Guo, S.; D. Powell, C.; Villagrán, D.; S. Wong, M. Magnetic In–Pd Catalysts for Nitrate Degradation. Environ. Sci. Nano 2020, 7 (9), 2681–2690. https://doi.org/10.1039/D0EN00069H.

(49) Levi, J.; Guo, S.; Kavadiya, S.; Luo, Y.; Lee, C.-S.; Jacobs, H. P.; Holman, Z.; Wong, M. S.; Garcia-Segura, S.; Zhou, C.; Rittmann, B. E.; Westerhoff, P. Comparing Methods to Deposit Pd-In Catalysts on Hydrogen-Permeable Hollow-Fiber Membranes for Nitrate Reduction. Water Res. 2023, 235, 119877. https://doi.org/10.1016/j.watres.2023.119877.

(50) Soares, O. S. G. P.; Órfão, J. J. M.; Pereira, M. F. R. Activated Carbon Supported Metal Catalysts for Nitrate and Nitrite Reduction in Water. Catal. Lett. 2008, 126 (3), 253–260. https://doi.org/10.1007/s10562-008-9612-4.

(51) Zhang, M.; Yan, Z.; Sun, Q.; Xie, J.; Jing, J. Synthetic Core–Shell Ni@Pd Nanoparticles Supported on Graphene and Used as an Advanced Nanoelectrocatalyst for Methanol Oxidation. New J. Chem. 2012, 36 (12), 2533. https://doi.org/10.1039/c2nj40651a.

(52) Metin, Ö.; Ho, S. F.; Alp, C.; Can, H.; Mankin, M. N.; Gültekin, M. S.; Chi, M.; Sun, S. Ni/Pd Core/Shell Nanoparticles Supported on Graphene as a Highly Active and Reusable Catalyst for Suzuki-Miyaura Cross-Coupling Reaction. Nano Res. 2013, 6 (1), 10–18. https://doi.org/10.1007/s12274-012-0276-4.

(53) She, Y.; Lu, Z.; Fan, W.; Jewell, S.; Leung, M. K. H. Facile Preparation of PdNi/rGO and Its Electrocatalytic Performance towards Formic Acid Oxidation. J. Mater. Chem. A 2014, 2 (11), 3894. https://doi.org/10.1039/c3ta14546h.

(54) Du, C.; Chen, M.; Wang, W.; Yin, G. Nanoporous PdNi Alloy Nanowires As Highly Active Catalysts for the Electro-Oxidation of Formic Acid. ACS Appl. Mater. Interfaces 2011, 3 (2), 105–109. https://doi.org/10.1021/am100803d.

(55) Zhang, M.; Ling, Y.; Liu, L.; Xu, J.; Li, J.; Fang, Q. Carbon Supported PdNi Alloy Nanoparticles on SiO 2 Nanocages with Enhanced Catalytic Performance. Inorg. Chem. Front. 2020, 7 (17), 3081–3091. https://doi.org/10.1039/D0QI00596G.

(56) Oh, S.-D.; Kim, M.-R.; Choi, S.-H.; Chun, J.-H.; Lee, K.-P.; Gopalan, A.; Hwang, C.-G.; Sang-Ho, K.; Hoon, O. J. Radiolytic Synthesis of Pd–M (M=Ag, Au, Cu, Ni and Pt) Alloy Nanoparticles and Their Use in Reduction of 4-Nitrophenol. J. Ind. Eng. Chem. 2008, 14 (5), 687–692. https://doi.org/10.1016/j.jiec.2008.04.008.

(57) Jiang, T.; Huai, Q.; Geng, T.; Ying, W.; Xiao, T.; Cao, F. Catalytic Performance of Pd–Ni Bimetallic Catalyst for Glycerol Hydrogenolysis. Biomass Bioenergy 2015, 78, 71–79. https://doi.org/10.1016/j.biombioe.2015.04.017.

(58) Insorn, P.; Kitiyanan, B. Selective Hydrogenation of Mixed C4 Containing High Vinyl Acetylene by Mn-Pd, Ni-Pd and Ag-Pd on Al2O3 Catalysts. Catal. Today 2015, 256, 223–230. https://doi.org/10.1016/j.cattod.2015.01.042.

(59) Trawczyński, J.; Gheek, P.; Okal, J.; Zawadzki, M.; Gomez, M. J. I. Reduction of Nitrate on Active Carbon Supported Pd-Cu Catalysts. Appl. Catal. Gen. 2011, 409–410, 39–47. https://doi.org/10.1016/j.apcata.2011.09.020.

(60) Zhang, X.; Liu, Y.; Ma, X.; Liu, X.; Zhang, R.; Wang, Y. Metal–Support Interaction of Carbon–Based Electrocatalysts for Oxygen Evolution Reaction. Nanoenergy Adv. 2023, 3 (1), 48–72. https://doi.org/10.3390/nanoenergyadv3010004.

(61) Baddour, F.; Van Allsburg, K.; Wunder, N.; Yarbrough, J.; Jankousky, M.; Gruchalla, K.; Potter, K.; Schaidle, J.; Tan, E.; Talmadge, M.; Hensley, J.; Habas, S.; Snowden-Swan, L.; Frye, J. CatCostTM (Catalyst Cost Estimation Tool) [SWR-18-74]. Computer Software. USDOE Office of Energy Efficiency and Renewable Energy (EERE), Bioenergy Technologies Office (EE-3B), 2019. https://doi.org/10.11578/DC.20191029.1.

(62) Halder, N. C.; Wagner, C. N. J. Separation of Particle Size and Lattice Strain in Integral Breadth Measurements. Acta Crystallogr. 1966, 20 (2), 312–313. https://doi.org/10.1107/S0365110X66000628.

(63) Rey, A.; Faraldos, M.; Bahamonde, A.; Casas, J. A.; Zazo, J. A.; Rodríguez, J. J. Role of the Activated Carbon Surface on Catalytic Wet Peroxide Oxidation. Ind. Eng. Chem. Res. 2008, 47 (21), 8166–8174. https://doi.org/10.1021/ie800538t.

(64) Snider, J. L.; Streibel, V.; Hubert, M. A.; Choksi, T. S.; Valle, E.; Upham, D. C.; Schumann, J.; Duyar, M. S.; Gallo, A.; Abild-Pedersen, F.; Jaramillo, T. F. Revealing the Synergy between Oxide and Alloy Phases on the Performance of Bimetallic In–Pd Catalysts for CO2 Hydrogenation to Methanol. ACS Catal. 2019, 9 (4), 3399–3412. https://doi.org/10.1021/acscatal.8b04848.

(65) Boitiaux, J. P.; Cosyns, J.; Vasudevan, S. Preparation and Characterisation of Highly Dispersed Palladium Catalysts on Low Surface Alumina, Their Notable Effects in Hydrogenation. Stud. Surf. Sci. Catal. 1983, 16, 123–124. https://doi.org/10.1016/S0167-2991(09)60015-X.

(66) Sheu, L. L.; Karpinski, Z.; Sachtler, W. M. H. Effects of Palladium Particle Size and

753 Palladium Silicide Formation on Fourier Transform Infrared Spectra and Carbon
754 Monoxide Adsorbed on Palladium/Silicon Dioxide Catalysts. J. Phys. Chem. 1989, 93
755 (12), 4890–4894. https://doi.org/10.1021/j100349a042.

756 (67) Fang, Y.-L.; Heck, K. N.; Alvarez, P. J. J.; Wong, M. S. Kinetics Analysis of
757 Palladium/Gold Nanoparticles as Colloidal Hydrodechlorination Catalysts. ACS Catal.
758 2011, 1 (2), 128–138. https://doi.org/10.1021/cs100067k.

759 (68) Zhang, R.; Shuai, D.; Guy, K. A.; Shapley, J. R.; Strathmann, T. J.; Werth, C. J.
760 Elucidation of Nitrate Reduction Mechanisms on a Pd-In Bimetallic Catalyst Using
761 Isotope Labeled Nitrogen Species. ChemCatChem 2013, 5 (1), 313–321.
762 https://doi.org/10.1002/cctc.201200457.

763 (69) Kresse, G.; Furthmüller, J. Efficient Iterative Schemes for Ab Initio Total-Energy
764 Calculations Using a Plane-Wave Basis Set. Phys. Rev. B 1996, 54 (16), 11169–11186.
765 https://doi.org/10.1103/PhysRevB.54.11169.

766 (70) Perdew, J. P.; Burke, K.; Ernzerhof, M. Generalized Gradient Approximation Made
767 Simple. Phys. Rev. Lett. 1996, 77 (18), 3865–3868.
768 https://doi.org/10.1103/PhysRevLett.77.3865.

769 (71) Kresse, G.; Joubert, D. From Ultrasoft Pseudopotentials to the Projector Augmented-
770 Wave Method. Phys. Rev. B 1999, 59 (3), 1758–1775.
771 https://doi.org/10.1103/PhysRevB.59.1758.

772 (72) Tran, R.; Xu, Z.; Radhakrishnan, B.; Winston, D.; Sun, W.; Persson, K. A.; Ong, S. P.
773 Surface Energies of Elemental Crystals. Sci. Data 2016, 3 (1), 160080.
774 https://doi.org/10.1038/sdata.2016.80.

775 (73) Monkhorst, H. J.; Pack, J. D. Special Points for Brillouin-Zone Integrations. Phys. Rev.
776 B 1976, 13 (12), 5188–5192. https://doi.org/10.1103/PhysRevB.13.5188.

777 (74) Neugebauer, J.; Scheffler, M. Adsorbate-Substrate and Adsorbate-Adsorbate
778 Interactions of Na and K Adlayers on Al(111). Phys. Rev. B 1992, 46 (24), 16067–16080.
779 https://doi.org/10.1103/PhysRevB.46.16067.

780 (75) Tang, W.; Sanville, E.; Henkelman, G. A Grid-Based Bader Analysis Algorithm without
781 Lattice Bias. J. Phys. Condens. Matter 2009, 21 (8), 084204.
782 https://doi.org/10.1088/0953-8984/21/8/084204.

783 (76) Baddour, F.; Van Allsburg, K.; Jankousky, M.; Wunder, N. CatCost™ Data Tools [SWR-
784 20-59]. Computer Software. USDOE Office of Energy Efficiency and Renewable Energy
785 (EERE), Transportation Office. Bioenergy Technologies Office, 2020.
786 https://doi.org/10.11578/dc.20201203.1.

787 (77) Boasiako, C. A.; Zhou, Z.; Huo, X.; Ye, T. Development of Pd-Based Catalysts for
788 Hydrogenation of Nitrite and Nitrate in Water: A Review. J. Hazard. Mater. 2023, 446,
789 130661. https://doi.org/10.1016/j.jhazmat.2022.130661.

790 (78) D'Arino, M.; Pinna, F.; Strukul, G. Nitrate and Nitrite Hydrogenation with Pd and
791 Pt/SnO2 Catalysts: The Effect of the Support Porosity and the Role of Carbon Dioxide in
792 the Control of Selectivity. Appl. Catal. B Environ. 2004, 53 (3), 161–168.
793 https://doi.org/10.1016/j.apcatb.2004.05.015.

794 (79) Clark, C. A.; Reddy, C. P.; Xu, H.; Heck, K. N.; Luo, G.; Senftle, T. P.; Wong, M. S.

Mechanistic Insights into pH-Controlled Nitrite Reduction to Ammonia and Hydrazine over Rhodium. ACS Catal. 2020, 10 (1), 494–509. https://doi.org/10.1021/acscatal.9b03239.

(80) Hörold, S.; Tacke, T.; Vorlop, K. Catalytical Removal of Nitrate and Nitrite from Drinking Water: 1. Screening for Hydrogenation Catalysts and Influence of Reaction Conditions on Activity and Selectivity. Environ. Technol. 1993, 14 (10), 931–939. https://doi.org/10.1080/09593339309385367.

(81) Ebbesen, S. D.; Mojet, B. L.; Lefferts, L. Effect of pH on the Nitrite Hydrogenation Mechanism over Pd/Al2O3 and Pt/Al2O3: Details Obtained with ATR-IR Spectroscopy. J. Phys. Chem. C 2011, 115 (4), 1186–1194. https://doi.org/10.1021/jp106521t.

(82) Krawczyk, N.; Karski, S.; Witońska, I. The Effect of Support Porosity on the Selectivity of Pd–In/Support Catalysts in Nitrate Reduction. React. Kinet. Mech. Catal. 2011, 103 (2), 311–323. https://doi.org/10.1007/s11144-011-0321-4.

(83) Pizarro, A. H.; Torija, I.; Monsalvo, V. M. Enhancement of Pd-Based Catalysts for the Removal of Nitrite and Nitrate from Water. J. Water Supply Res. Technol. 2018, 67 (7), 615–625. https://doi.org/10.2166/aqua.2018.024.

(84) Venezia, A. M.; Rossi, A.; Duca, D.; Martorana, A.; Deganello, G. Particle Size and Metal-Support Interaction Effects in Pumice Supported Palladium Catalysts. Appl. Catal. Gen. 1995, 125 (1), 113–128. https://doi.org/10.1016/0926-860X(94)00286-X.

(85) Kumar, G.; Blackburn, J. R.; Albridge, R. G.; Moddeman, W. E.; Jones, M. M. Photoelectron Spectroscopy of Coordination Compounds. II. Palladium Complexes. Inorg. Chem. 1972, 11 (2), 296–300. https://doi.org/10.1021/ic50108a020.

(86) Levi, J.; Jung, B.; Jacobs, H. P.; Luo, Y.; Lee, C.-S.; Hong, K.; Long, M.; Donoso, J.; Garcia-Segura, S.; Wong, M. S.; Rittmann, B. E.; Westerhoff, P. Optimized Bimetallic Ratios for Durable Membrane Catalyst-Film Reactors in Treating Nitrate-Polluted Water. Sci. Total Environ. 2024, 943, 173711. https://doi.org/10.1016/j.scitotenv.2024.173711.

(87) Faur, M.; Faur, M.; Jayne, D. T.; Goradia, M.; Goradia, C. XPS Investigation of Anodic Oxides Grown on P-Type InP. Surf. Interface Anal. 1990, 15 (11), 641–650. https://doi.org/10.1002/sia.740151102.

(88) Detweiler, Z. M.; Wulfsberg, S. M.; Frith, M. G.; Bocarsly, A. B.; Bernasek, S. L. The Oxidation and Surface Speciation of Indium and Indium Oxides Exposed to Atmospheric Oxidants. Surf. Sci. 2016, 648, 188–195. https://doi.org/10.1016/j.susc.2015.10.026.

(89) Xie, J.-X.; Cao, J.-P.; Zhao, X.-Y.; Jiang, W.; Zhao, L.; Zhao, M.; Bai, H.-C. Selective Cleavage of the Diphenyl Ether C–O Bond over a Ni Catalyst Supported on AC with Different Pore Structures and Hydrophilicities. Energy Fuels 2021, 35 (11), 9599–9608. https://doi.org/10.1021/acs.energyfuels.1c00809.

(90) Shin, H.; Jung, S.; Bae, S.; Lee, W.; Kim, H. Nitrite Reduction Mechanism on a Pd Surface. Environ. Sci. Technol. 2014, 48 (21), 12768–12774. https://doi.org/10.1021/es503772x.

(91) Zhao, Y.; Koteswara Rao, N.; Lefferts, L. Adsorbed Species on Pd Catalyst during Nitrite Hydrogenation Approaching Complete Conversion. J. Catal. 2016, 337, 102–110. https://doi.org/10.1016/j.jcat.2016.02.007.

(92) Sharma, V.; Sharma, S.; Sharma, N.; Sharma, S.; Paul, S. A Novel Core–Shell Pd(0)@enSiO 2 –Ni–TiO 2 Nanocomposite with a Synergistic Effect for Efficient Hydrogenations. New J. Chem. 2022, 46 (35), 16959–16969. https://doi.org/10.1039/D2NJ02845J.

(93) Zhang, Z.; Shi, W.; Wang, W.; Xu, Y.; Bao, X.; Zhang, R.; Zhang, B.; Guo, Y.; Cui, F. Interfacial Electronic Effects of Palladium Nanocatalysts on the By-Product Ammonia Selectivity during Nitrite Catalytic Reduction. Environ. Sci. Nano 2018, 5 (2), 338–349. https://doi.org/10.1039/C7EN00909G.

847 Table of Contents (TOC) image

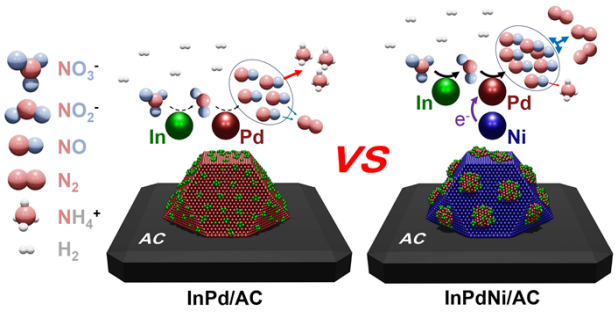

848